JOURNAL OF GUIDANCE, CONTROL, AND DYNAMICS
Vol. 25, No. 5, September–October 2002

Model Predictive Lateral Pulse Jet Control of an Atmospheric Rocket

Bradley Burchett* and Mark Costello†
Oregon State University, Corvallis, Oregon 97331

Uncontrolled direct fire atmospheric rockets exhibit high impact point dispersion, even at relatively short range, and, as such, have been employed as area weapons on the battlefield. To reduce the dispersion of a direct fire rocket, the use of a small number of short-duration lateral pulses acting as a control mechanism is investigated. A unique control law is reported that combines model predictive control and linear projectile theory for lateral pulse jet control of an atmospheric rocket. The impact point in the target plane is directly controlled. Through simulation, this model predictive flight control law is shown to efficiently reduce direct fire rocket dispersion. A parametric trade study on an example rocket configuration is reported that details the effect of the number and amplitude of individual pulse jets, as well as the effect of the flight control system computation cycle time.

Nomenclature

C_{mq}	=	pitch rate damping moment aerodynamic coefficient
C_{NA}	=	normal force aerodynamic coefficient
D	=	projectile characteristic length
I_{xx}, I_{yy}	=	roll and pitch inertia
L, M, N	=	total external applied moment on the rocket about the mass center expressed in the rocket reference frame
m	=	projectile mass
p, q, r	=	angular velocity vector components expressed in the fixed plane reference frame
R_{Ix}	=	projectile axis of symmetry component of vector from body mass center to the impulse application point
r_m	=	switching surface radius at the target
SL_{cg}	=	stationline of the projectile c.g. location
SL_{cp}	=	stationline of the projectile c.p. location
S_l	=	taper ratio of switching surface
S_P	=	slope of a line segment from the target to the predicted uncontrolled impact point
S_W	=	radius of switching surface at current range
u, v, w	=	translation velocity components of the projectile center of mass resolved in the fixed plane reference frame
V	=	magnitude of the mass center velocity
X, Y, Z	=	total external applied force on the rocket expressed in the rocket reference frame
x, y, z	=	position vector components of the projectile mass center expressed in the inertial reference frame
x_I, y_I, z_I	=	position vector components of the linear model predicted impact point without control
x_I^*, y_I^*, z_I^*	=	position vector components of the linear model predicted impact point with control
x_T, y_T, z_T	=	position vector components of the target expressed in the inertial reference frame
Y_J, Z_J	=	pulse jet force components in the rocket reference frame
γ	=	counterclockwise angle in inertial space from Z axis to vector from current predicted impact point to target
ε	=	current miss distance
ζ	=	angle from the rocket z axis counterclockwise to the line of action of nth pulse force as seen from aft of the rocket
$\theta_{\alpha f}, \theta_{\alpha s}$	=	phase angles of the fast and slow epicyclic modes
λ_f, λ_s	=	fast and slow epicyclic mode damping factors
ξ_i, η_i^T	=	ith epicyclic mode right and left eigenvectors
ρ	=	air density
Φ_f, Φ_s	=	fast and slow epicyclic mode damped natural frequencies
ψ, θ, ϕ	=	Euler yaw, pitch, and roll angles
$\Omega_{\alpha f}, \Omega_{\alpha s}$	=	amplitudes of the fast and slow epicyclic modes

Introduction

DIRECT fire atmospheric rockets are fired by line-of-sight aiming and are fired from ground-based platforms, helicopters, and fixed-wing aircraft. These rockets exit the launcher with low speed. Any aerodynamic disturbances presented to the rocket near the launcher create relatively large aerodynamic angles of attack, leading to increased target dispersion. Furthermore, main rocket motor thrust during the initial portion of flight tends to amplify significantly the effect of transverse and angular velocity perturbations on initial disturbances as the rocket enters atmospheric flight. With the advent of low-cost, small, rugged, microelectomechanical systems, dramatic reduction of dispersion for direct fire rockets equipped with a relatively inexpensive flight control system is possible. One design concept consists of a ring of lateral pulse jets mounted near the nose of the rocket. This paper develops a unique flight control law tailored to lateral pulse jet control of smart projectiles through the application of model predictive control and linear projectile theory.

In model predictive control, a dynamic model of the plant is used to project the state into the future and subsequently use the estimated future state to determine control action. It has been found to be a practical and powerful control technique in industrial control when future reference states are known.[1] A key element of any model predictive control scheme is the underlying dynamic model representing the plant. The equations of motion for a rocket in atmospheric flight can be adequately represented under most flight conditions by a rigid body possessing six degrees of freedom. In the literature, significant attention has been paid to manipulation and simplification of the equations of motion to allow closed-form solution of the ballistic trajectory of a projectile under restricted flight conditions. The resulting dynamic equations and the resulting solutions

Received 9 July 2001; revision received 11 January 2002; accepted for publication 18 April 2002.

*Graduate Research Assistant, Department of Mechanical Engineering. Member AIAA.

†Assistant Professor, Department of Mechanical Engineering. Member AIAA.

have become known as projectile linear theory. Over time, projectile linear theory has been extended by various authors to handle more sophisticated aerodynamic models,[2] asymmetric mass properties,[3] fluid payloads,[4,5] moving internal parts,[6,7] dual spin projectiles,[8,9] ascending flight,[10] and lateral force impulses.[11–13] Aerodynamic range reduction software used in spark range facilities utilizes projectile linear theory in estimation of aerodynamic coefficients.

A large collection of literature has accumulated in the area of missile flight control, and standard control system design techniques have been established. Details on these methods are provided by, for example, Zarchan.[14] Generally, these control system design techniques have been established for missile configurations with a continuous control mechanism. In the case of a lateral pulse jet control mechanism, a small number of individual impulse thrusters are fired to affect control. Each impulse thruster delivers a large, short-duration impulse to the body in the lateral direction. This control mechanism falls out of the normal realm of continuous or discrete control where control authority is possible during the entire trajectory and into the category of impulse control. General pulse control techniques have been developed, particularly in the electronics industry, for pulse width and pulse frequency modulation. These methods have been optimized for simple low-order plants.[15–20] Pulse control concepts have also been employed to control spacecraft.[21–27] Harkins and Brown[28] considered the use of a set of lateral pulse jets to reduce dispersion of a rocket by firing pulse jets to minimize projectile pitch and yaw rate. For the notional cases evaluated, dispersion was reduced by a factor of five. Jitpraphai and Costello[29] used a trajectory tracking flight control system to improve impact point performance of a direct fire rocket equipped with a ring of lateral pulse jets. For the guidance technique employed, dispersion reduction was found to be strongly dependent on pulse jet magnitude and tracking window size.

The work reported hereafter employs model predictive controller and projectile linear theory specialized to lateral pulse jet control of a direct fire atmospheric rocket. The basic rocket configuration under consideration is fin stabilized and the fins are slightly canted to provide moderate roll rates during flight. A ring of lateral pulse jets mounted on the skin of the rocket near the nose is used as the control actuator. Each individual pulse jet imparts a relatively large- and short-duration lateral force on the projectile body. Each pulse jet can fire only once, and the pulse jets cannot be reloaded. The control law uses an approximate closed-form solution of projectile motion to map the current state of the rocket to the target plane, allowing direct control of the impact point. Pulse jet firing logic is based on the difference between the target and the estimated impact point. Projectile linear theory is the basic building block for predicting the impact point of a projectile from an arbitrary state, both with and without firing of lateral pulse jets. The rocket is not roll controlled. Also, it is assumed that sensor feedback is provided by an onboard inertial measurement unit (IMU). Simulation results to establish the utility of the new lateral pulse jet predictive flight control system design methodology are generated for an exemplar direct fire rocket. Parametric trade studies are conducted that consider the effect of the number of pulse jets, impulse magnitude, and control system cycle time on impact point dispersion.

Projectile Dynamic Model

The nonlinear trajectory simulation used in this study is a standard six-degree-of-freedom model typically used in flight dynamic modeling of projectiles. A schematic of the rocket configuration is shown in Figs. 1 and 2. The six degrees of freedom are the three inertial components of the position vector from an inertial frame to the rocket mass center and the three standard Euler orientation angles. The equations of motion are provided in Eqs. (1–4) (Refs. 30–32):

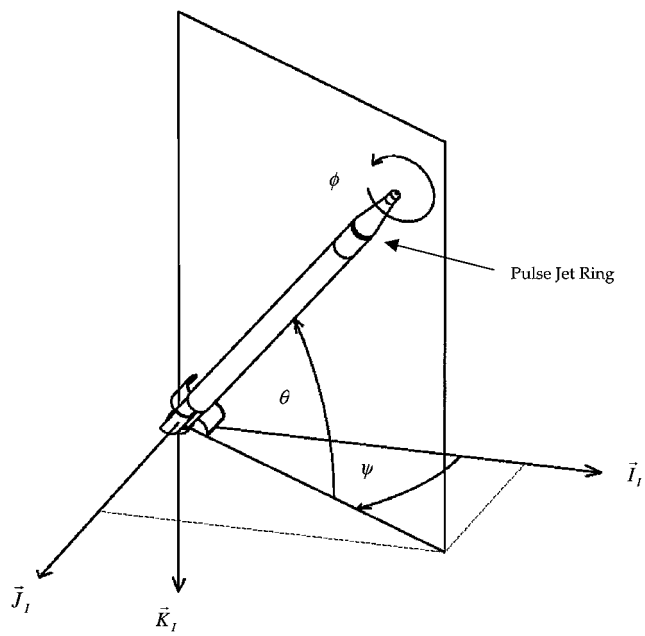

Fig. 2 Schematic of the attitude coordinates of a direct fire rocket.

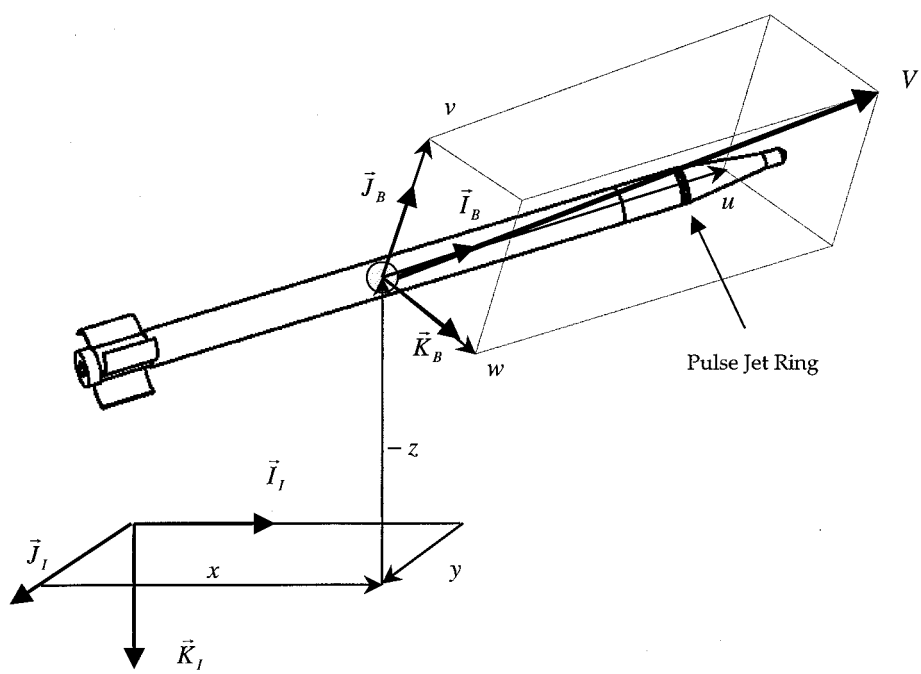

Fig. 1 Schematic of the position coordinates of a direct fire rocket.

$$\begin{Bmatrix}\dot{x}\\ \dot{y}\\ \dot{z}\end{Bmatrix}=\begin{bmatrix}c_\theta c_\psi & s_\phi s_\theta c_\psi - c_\phi s_\psi & c_\phi s_\theta c_\psi + s_\phi s_\psi\\ c_\theta s_\psi & s_\phi s_\theta s_\psi + c_\phi c_\psi & c_\phi s_\theta s_\psi - s_\phi c_\psi\\ -s_\theta & s_\phi c_\theta & c_\phi c_\theta\end{bmatrix}\begin{Bmatrix}u\\ v\\ w\end{Bmatrix} \quad (1)$$

$$\begin{Bmatrix}\dot{\phi}\\ \dot{\theta}\\ \dot{\psi}\end{Bmatrix}=\begin{bmatrix}1 & s_\phi t_\theta & c_\phi t_\theta\\ 0 & c_\phi & -s_\phi\\ 0 & s_\phi/c_\theta & c_\phi/c_\theta\end{bmatrix}\begin{Bmatrix}p\\ q\\ r\end{Bmatrix} \quad (2)$$

$$\begin{Bmatrix}\dot{u}\\ \dot{v}\\ \dot{w}\end{Bmatrix}=\begin{Bmatrix}X/m\\ Y/m\\ Z/m\end{Bmatrix}-\begin{bmatrix}0 & -r & q\\ r & 0 & -p\\ -q & p & 0\end{bmatrix}\begin{Bmatrix}u\\ v\\ w\end{Bmatrix} \quad (3)$$

$$\begin{Bmatrix}\dot{p}\\ \dot{q}\\ \dot{r}\end{Bmatrix}=[I]^{-1}\left[\begin{Bmatrix}L\\ M\\ N\end{Bmatrix}-\begin{bmatrix}0 & -r & q\\ r & 0 & -p\\ -q & p & 0\end{bmatrix}[I]\begin{Bmatrix}p\\ q\\ r\end{Bmatrix}\right] \quad (4)$$

In Eqs. (1) and (2), the standard shorthand notation for trigonometric functions is used: $\sin(\alpha)\equiv s_\alpha$, $\cos(\alpha)\equiv c_\alpha$, and $\tan(\alpha)\equiv t_\alpha$. The forces appearing in Eq. (3) contain contributions from weight W, body aerodynamics A, main rocket thrust R, and the lateral pulse jets J:

$$\begin{Bmatrix}X\\ Y\\ Z\end{Bmatrix}=\begin{Bmatrix}X_W\\ Y_W\\ Z_W\end{Bmatrix}+\begin{Bmatrix}X_A\\ Y_A\\ Z_A\end{Bmatrix}+\begin{Bmatrix}X_R\\ Y_R\\ Z_R\end{Bmatrix}+\begin{Bmatrix}X_J\\ Y_J\\ Z_J\end{Bmatrix} \quad (5)$$

The dynamic equations are expressed in a body-fixed reference frame, thus, all forces acting on the body are expressed in the rocket reference frame. The rocket weight force is shown in Eq. (6):

$$\begin{Bmatrix}X_W\\ Y_W\\ Z_W\end{Bmatrix}=mg\begin{Bmatrix}-s_\theta\\ s_\phi c_\theta\\ c_\phi c_\theta\end{Bmatrix} \quad (6)$$

whereas the aerodynamic force acting at the center of pressure of the rocket is given by Eq. (7):

$$\begin{Bmatrix}X_A\\ Y_A\\ Z_A\end{Bmatrix}=-\frac{\pi}{8}\rho V^2 D^2\begin{Bmatrix}C_{X0}+C_{X2}(v^2+w^2)/V^2\\ C_{NA}v/V\\ C_{NA}w/V\end{Bmatrix} \quad (7)$$

The main rocket motor increases the velocity of the rocket by providing high thrust levels during the initial portion of the trajectory:

$$\begin{Bmatrix}X_R\\ Y_R\\ Z_R\end{Bmatrix}=T_R\begin{Bmatrix}n_{RX}\\ n_{RY}\\ n_{RZ}\end{Bmatrix} \quad (8)$$

In Eq. (8), the thrust amplitude profile T_R is a known function of time. The lateral pulse jet forces are modeled in the same manner as the main rocket motor, with two exceptions. Because the lateral pulse jets are active over a very short duration of time when compared to the timescale of a complete rocket trajectory, the thrust force is modeled as a constant when active. Also, because, by definition, a lateral pulse jet acts in the $\boldsymbol{j}_B$ and $\boldsymbol{k}_B$ plane, the $\boldsymbol{i}_B$ component of the lateral pulse jet force is zero. Equation (9) provides the lateral pulse jet force formula:

$$\begin{Bmatrix}X_J\\ Y_J\\ Z_J\end{Bmatrix}=\sum_{i=1}^{n_J}T_{Ji}\begin{Bmatrix}0\\ -\cos[2\pi(i-1)/n_J]\\ -\sin[2\pi(i-1)/n_J]\end{Bmatrix} \quad (9)$$

The pulse jet ring is located on the skin of the projectile and near the nose of the rocket. Individual pulse jets are uniformly distributed azimuthally around the lateral pulse jet ring. A key feature of the pulse jet configuration considered here is that each pulse jet can be fired only once.

The applied moments about the rocket mass center contains contributions from steady aerodynamics (SA), unsteady aerodynamics (UA), main rocket thrust R, and lateral pulse jets J:

$$\begin{Bmatrix}L\\ M\\ N\end{Bmatrix}=\begin{Bmatrix}L_{\mathrm{SA}}\\ M_{\mathrm{SA}}\\ N_{\mathrm{SA}}\end{Bmatrix}+\begin{Bmatrix}L_{\mathrm{UA}}\\ M_{\mathrm{UA}}\\ N_{\mathrm{UA}}\end{Bmatrix}+\begin{Bmatrix}L_R\\ M_R\\ N_R\end{Bmatrix}+\begin{Bmatrix}L_J\\ M_J\\ N_J\end{Bmatrix} \quad (10)$$

The moment components due to steady aerodynamic forces, main rocket motor forces, and lateral pulse jet forces are computed with a cross product between the distance vector from the mass center of the rocket and the location of the specific force and the force itself. The unsteady body aerodynamic moment provides a damping source for projectile angular motion and is given by Eq. (11):

$$\begin{Bmatrix}L_{\mathrm{UA}}\\ M_{\mathrm{UA}}\\ N_{\mathrm{UA}}\end{Bmatrix}=\frac{\pi}{8}\rho V^2 D^3\begin{Bmatrix}C_{DD}+\dfrac{pDC_{\mathrm{LP}}}{2V}\\ \dfrac{qDC_{\mathrm{mq}}}{2V}\\ \dfrac{rDC_{\mathrm{mq}}}{2V}\end{Bmatrix} \quad (11)$$

When the rocket motor is active, the mass, mass center location, and inertial properties of the rocket are updated continuously. The center of pressure location and all aerodynamic coefficients (C_{X0}, C_{X2}, C_{NA}, C_{DD}, C_{LP}, and C_{mq}) depend on local Mach number and are computed during simulation using linear interpolation.

The dynamic equations given by Eqs. (1–4) are numerically integrated forward in time using a fourth-order, fixed-step Runge–Kutta algorithm. Costello and Anderson[33] present correlation of this dynamic model against range data for a fin stabilized projectile.

Projectile Linear Theory Trajectory Solution

The six degree of freedom projectile model just shown consists of 12 highly nonlinear differential equations that are not directly amenable to a closed-form solution. Over the past 60 years, ballisticians have investigated simplifications to the equations of motion, which yield an accurate, yet analytically solvable, set of equations. The resulting theory that has emerged is commonly called projectile linear theory.[31,32] Projectile linear theory is used to compute rapidly projectile trajectories, to reduce aerodynamic range data, and to establish stability criteria for both fin- and spin-stabilized projectiles. It is generally accepted as an accurate dynamic model for a wide class of fin- and spin-stabilized projectiles. Rather than employing a reference frame fixed to the projectile body, projectile linear theory uses an intermediate reference frame that is aligned with the projectile axis of symmetry, but that does not roll. Dimensionless arc length s is used as the independent variable instead of time t. Also, a change of variables is made from the velocity along the projectile axis of symmetry u to the total velocity V. Moreover, Euler pitch and yaw angles, as well as aerodynamic angle of attack, are assumed to be small. A more detailed discussion of the development of projectile linear theory is provided by McCoy.[31] The linear theory trajectory solution is provided in Eqs. (12) and (13):

$$\begin{aligned}\frac{y(s)}{D}=&\frac{y_0}{D}+\left(\psi_0+\frac{v_0}{V_0}\right)s\\ &+\left[\frac{\rho SD}{2m}\right]\frac{(C_{X0}-C_{\mathrm{NA}})}{V_0}\left\{\frac{\Omega_{vf}}{\phi_f^2}\left[\exp\left(\lambda_f^* s\right)\sin(\phi_f s+\theta_{vf}-\pi)\right.\right.\\ &\left.\left.-\sin(\theta_{vf}-\pi)-\phi_f\cos(\theta_{vf}-\pi)s\right]\right\}\\ &+\left[\frac{\rho SD}{2m}\right]\frac{(C_{X0}-C_{\mathrm{NA}})}{V_0}\left\{\frac{\Omega_{vs}}{\phi_s^2}\left[\exp\left(\lambda_s^* s\right)\sin(\phi_s s+\theta_{vs}-\pi)\right.\right.\\ &\left.\left.-\sin(\theta_{vs}-\pi)-\phi_s\cos(\theta_{vs}-\pi)s\right]\right\}\end{aligned} \quad (12)$$

$$\frac{z(s)}{D} = \frac{z_0}{D} + \left(-\theta_0 + \frac{w_0}{V_0}\right)s + gD\left[\frac{m}{\rho SDV_0C_{X0}}\right]^2 \times \left\{\exp\left(\left[\frac{\rho SD}{m}\right]C_{X0}s\right) - \left[\frac{\rho SD}{m}\right]C_{X0}s - 1\right\} + \left[\frac{\rho SD}{2m}\right]\frac{(C_{X0} - C_{NA})}{V_0}\left\{\frac{\Omega_{wf}}{\phi_f^2}\left[\exp\left(\lambda_f^* s\right)\sin(\phi_f s + \theta_{wf} - \pi) - \sin(\theta_{wf} - \pi) - \phi_f\cos(\theta_{wf} - \pi)s\right]\right\} + \left[\frac{\rho SD}{2m}\right]\frac{(C_{X0} - C_{NA})}{V_0}\left\{\frac{\Omega_{ws}}{\phi_s^2}\left[\exp\left(\lambda_s^* s\right)\sin(\phi_s s + \theta_{ws} - \pi) - \sin(\theta_{ws} - \pi) - \phi_s\cos(\theta_{ws} - \pi)s\right]\right\} \quad (13)$$

This trajectory solution contains constant terms, proportional terms, and damped sinusoid terms. The constant term depends on the initial location of the projectile. The proportional terms depend on the initial Euler angles and the initial crossing velocity of the projectile. The damped sinusoid terms depend on a set of constants that, in turn, depend on the initial state of the projectile. Costello and Peterson[34] provide definitions for the constants Ω_{vf}, Ω_{vs}, λ_f^*, λ_s^*, ϕ_f, ϕ_s, θ_{vf}, θ_{vs}, Ω_{wf}, Ω_{ws}, θ_{wf}, and θ_{ws}.

The projectile linear theory solution is used within the flight control system to predict the impact point of the rocket from a given state of the system, which is obtained in flight from the IMU. The accuracy of the linear projectile theory trajectory solution is improved if a piecewise solution is constructed. This is accomplished by discretizing the downrange distance from the current state to the target. The trajectory is computed by marching forward in arc length along the discretized segments. At each segment, the aerodynamic coefficients are updated based on the predicted Mach number at the segment. The effect of a lateral impulsive force can also be included in the trajectory solution by introducing a discontinuity in projectile crossing velocity v and w and angular rates q and r (Ref. 13). Because the model constants Ω_{vf}, Ω_{vs}, λ_f^*, λ_s^*, ϕ_f, ϕ_s, ϕ_{vf}, ϕ_{vs}, Ω_{wf}, Ω_{ws}, θ_{wf}, and θ_{ws} depend on the initial state of the projectile, they must be updated directly after a pulse is fired.

Predictive Flight Control System

The predictive flight control law uses projectile linear theory to transform the task of controlling the projectile over the trajectory into one of controlling the impact point in the target plane. Control input is based on a two-dimensional comparison of the commanded target location vs the predicted impact point in cross range and altitude. Figure 3 illustrates the flight control law in a block diagram form.

It is assumed that full state feedback is available for use in the control law, that is, x, y, z, ψ, θ, ϕ, u, v, w, p, q, and r have been sensed or estimated by the IMU. Furthermore, the weapon that fires the projectile has provided inertial coordinates of the target, x_T, y_T, z_T. At each cycle of the flight control system, the current time, projectile state, and downrange location of the target are input to the impact point estimator. The impact point estimator uses projectile linear theory to compute the impact point from the current state of the projectile. Note that the controller is taking into account the entire current state of the projectile, not just position. The miss distance ε is then estimated from the magnitude of the difference between the predicted impact point and the known target location. The miss distance formula is provided by Eq. (14):

$$\varepsilon = \sqrt{(y_T - y_I)^2 + (z_T - z_I)^2} \quad (14)$$

Based on this geometry, the miss distance phase angle γ is defined as the angle from the z axis counterclockwise to the required pulse direction, as seen from aft of the projectile:

$$\gamma = -\tan^{-1}\left(\frac{y_T - y_I}{z_T - z_I}\right) \quad (15)$$

The radius S_W is a circular window around the target into which the control law seeks to drive the projectile impact point. The window S_W is a linear function of downrange position. As the projectile flies downrange, the window S_W becomes smaller. The firing decision block compares the miss distance with S_W. If the miss distance is greater than S_W, then a pulse firing time is computed. In this case, the flag i_{fire} is set to 1, and the flight control system computes a pulse jet firing time for the next unfired individual lateral pulse jet motor.

Figure 4 provides a block diagram of the pulse jet firing logic. The proposed pulse jet firing time is generated by computing the change in projectile roll angle needed to align the lateral control force with the impact point error angle γ. Because the roll angle and roll rate are approximately related by $\phi = pt$, the difference between the firing time of the ith pulse jet and the current time is $t = \Delta\phi/p$. Equation (16) provides the formula for Δt_{fire}:

$$\Delta t_{\text{fire}} = (\gamma - \zeta_i - 2\pi - \phi_{\text{curr}})/p \quad (16)$$

For a fin-stabilized projectile with the lateral pulse jet ring mounted forward of the mass center, the change in impact point due to firing a pulse jet is approximately in the same direction as the applied lateral pulse jet force. By firing a pulse jet at $t + \Delta t_{\text{fire}}$, the pulse jet changes the impact point in the direction of the target. This is shown in Fig. 5.

With the current time, projectile state, and the proposed time until the ith pulse jet is fired, the impact point estimator uses projectile linear theory to estimate the impact point, which includes the effect of firing the ith pulse jet at time $t + \Delta t_{\text{fire}}$. The impact point is denoted with an asterisk superscript. Then, by the use of the impact point with and without the ith pulse jet fired and the target location, the

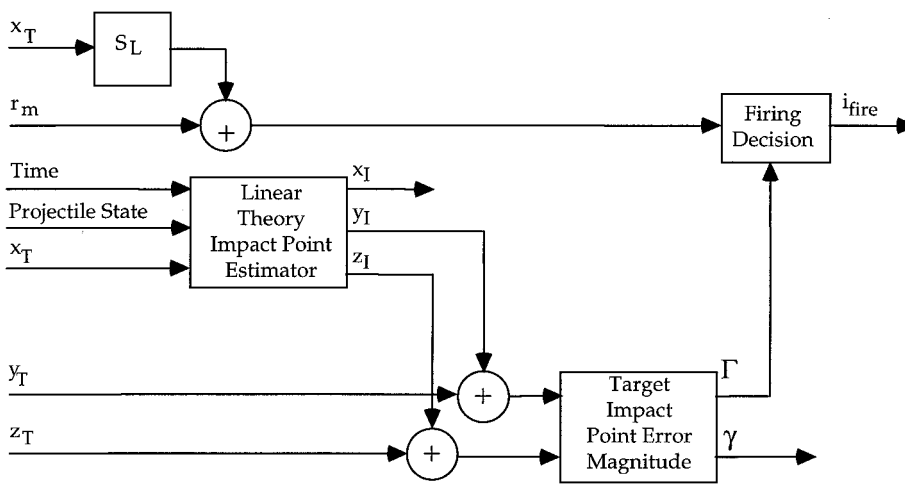

Fig. 3 Predictive impact point flight control system.

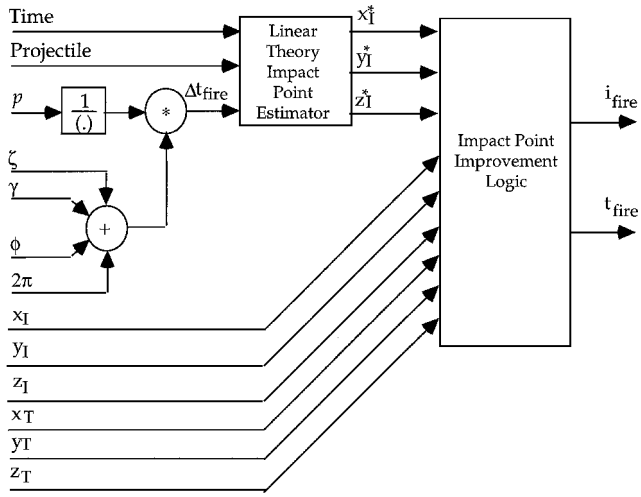

Fig. 4 Pulse jet firing logic.

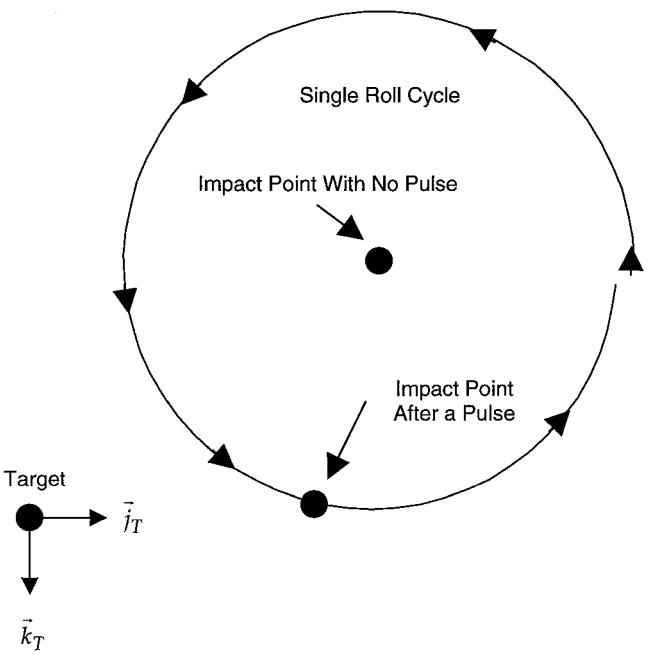

Fig. 5 Set of achievable impact points in the target plane due to a single pulse.

impact point improvement logic determines if the pulse jet should be fired. The purpose of the pulse jet improvement logic is to establish the extent to which the impact point will be improved. Figure 6 depicts the basic scenario. The allowable overshoot radius permits a pulse to overshoot the target by a percentage of the current miss distance.

The contour of impact points for admissible pulses is simply a line perpendicular to the desired pulse direction combined with a circle of permissible overshoot. That is, the pulse will be expended if the impact point is predicted to move anywhere on the same side of the target as the uncontrolled impact point, or anywhere within a specified overshoot ring.

The logic to ensure the pulse drives the projectile closer to the target is as follows. First, the slope of a line segment from the target to the predicted uncontrolled impact point is computed:

$$S_p = (y_I - y_T)/(z_I - z_T) \tag{17}$$

Equations (18) and (19) provide two inequalities. If both conditions are true or both conditions are false, then both points are on the same side of the overshoot line and the pulse jet is fired:

$$y_I \geq [(y_T - 1)/S_P](z_I - z_T) \tag{18}$$

Table 1 Parameters for typical controlled trajectory

Pulse number	Time at pulse, s	Range at pulse, ft	Roll angle, deg	Total angle, deg
1	1.0712	1325.4	133.5	133.5
2	1.2889	1796.9	106.4	134.1
3	1.2969	1814.0	78.5	133.9
4	1.4107	2054.7	50.8	133.9
5	1.6425	2534.2	22.0	132.8
6	1.7709	2793.6	−5.7	132.7
7	2.0387	3320.9	−34.6	131.5
8	2.1892	3609.2	−62.3	131.6
9	2.2006	3630.8	−90.6	130.9
10	2.3610	3931.7	−118.6	130.7
11	3.2865	5554.8	−147.4	129.5
12	5.3574	8633.1	−171.8	132.8

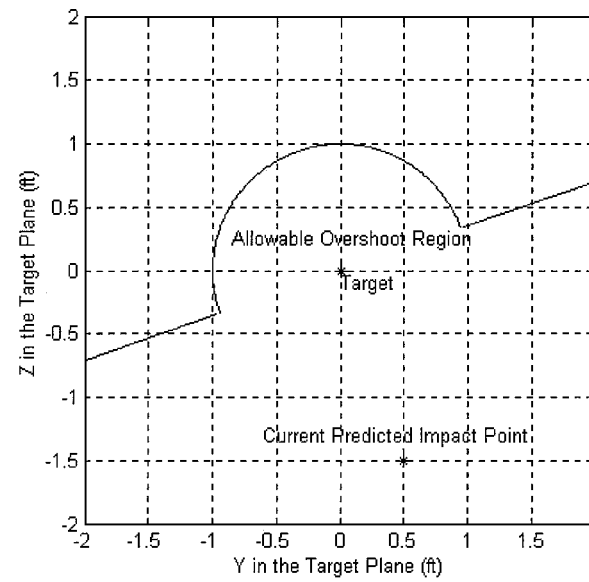

Fig. 6 Geometry of allowable overshoot region.

$$y_I^* \geq [(y_T - 1)/S_P]\left(z_I^* - z_T\right) \tag{19}$$

The asterisk denotes controlled impact point coordinates. Finally, a controlled miss distance is calculated using Eq. (14). If this computed miss distance is less than the allowable overshoot, the pulse will be expended regardless of the outcome of Eqs. (18) and (19).

Results

The example projectile considered for establishing the utility of the proposed control law is a 4.5-ft-long fin-stabilized projectile with a total weight of 23.0 lbf and a center of gravity location of 2.5 ft from the base. The projectile has three fins. The roll and pitch inertia of the body is 0.005 and 1.4 slug · ft^2, respectively. The main motor provides a constant thrust of 1600 lb from $t = 0.05$ to 0.95 s with startup and burnout modeled as linear ramps from $t = 0$ to 0.05 and from 0.95 to 1 s, respectively. An array of lateral pulse jets is located a distance of 3.80 ft from the projectile base on the skin of the projectile.

Table 1 and Figs. 7–10 illustrate a typical controlled trajectory due to an array of 12 2.25 lbf · s pulses. The rocket is launched with the following initial conditions: x_0, y_0, z_0, ϕ_0, ψ_0, v_0, w_0, and $p_0 = 0$. $\theta_0 = 4.58$ deg, $V_0 = 100$ ft/s, $q_0 = -17.75$ deg/s, and $r_0 = 10.56$ deg/s. The controller parameters for this trajectory were set such that the controller does not command pulse jet firing during the powered portion of flight. This is indicated by the initial trend of cross range that causes a large miss if no control action is exercised. The 12 pulses are fired at the times indicated in Table 1, resulting in bending of the cross range trajectory such that the projectile impacts approximately 2 ft from the target. Table 1 shows the time, range, and roll angle at which each pulse is fired. The final column of Table 1 displays the total clockwise angle from Earth-fixed $Y(J)$

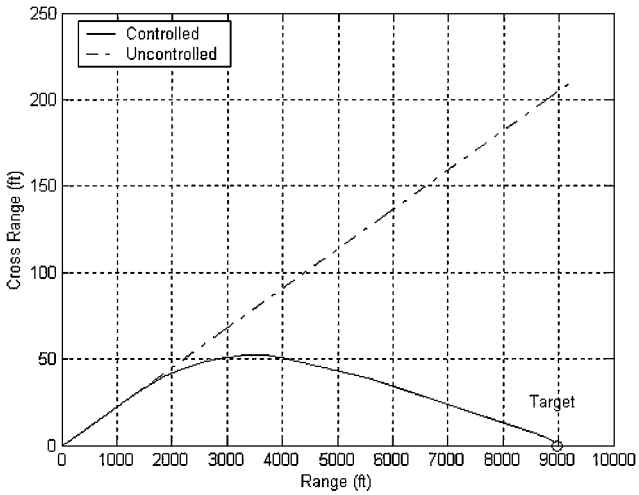

Fig. 7 Cross range vs range: typical controlled trajectory.

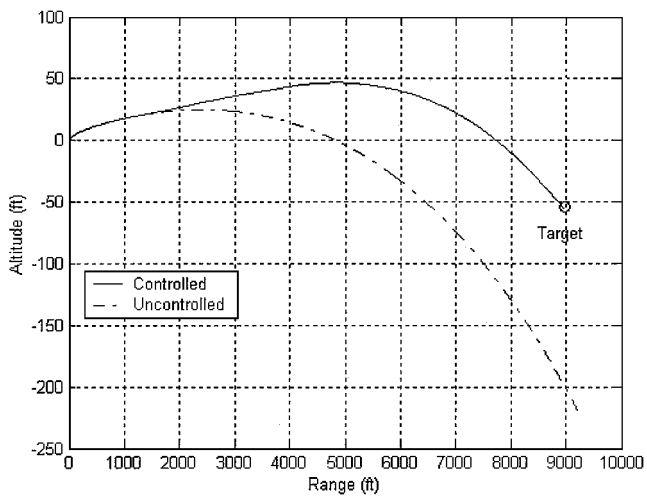

Fig. 8 Altitude vs range: typical controlled trajectory.

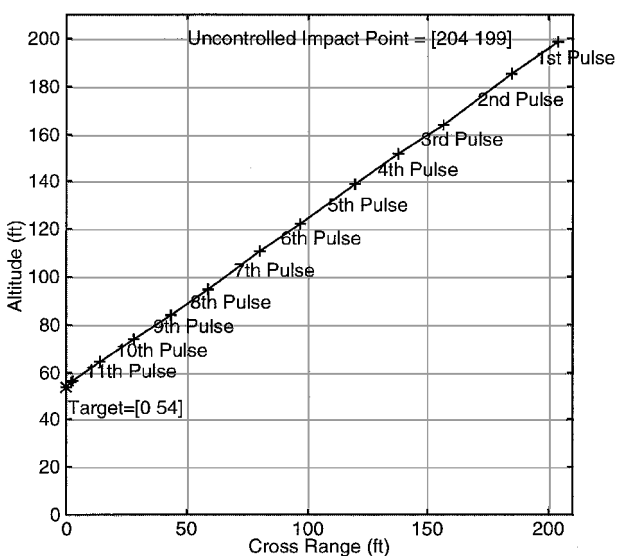

Fig. 9 Evolution of projectile impact point.

axis at which the pulse force was directed. Figure 7 shows the cross range vs range, whereas Fig. 8 displays the altitude profile for this typical controlled trajectory. The fixed target is located 54 ft below the launcher. Figure 9 shows the projectile impact point for the uncontrolled case and trajectories controlled by arrays of 1–12 pulses. The impact points are displayed as black crosses. The pulse labels refer to the line segments between impact points, which represent the correction due to each respective pulse. In each case, adding a

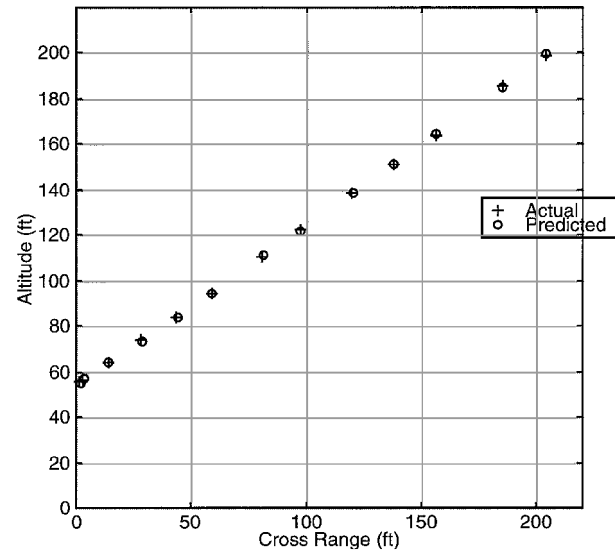

Fig. 10 Evolution of projectile impact point, with prediction of controlled impact point.

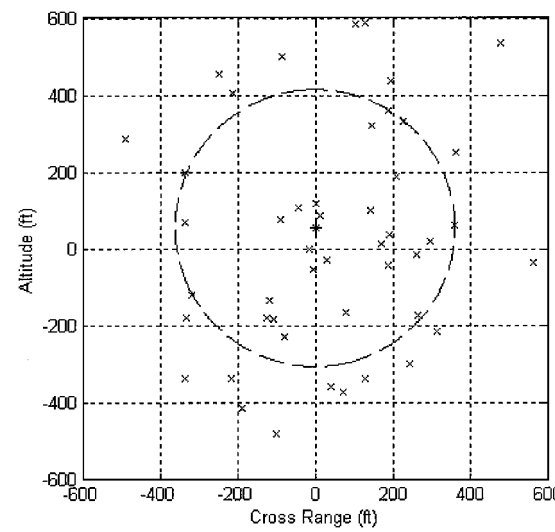

Fig. 11 Uncontrolled dispersion (CEP = 360.7 ft).

pulse takes the final impact point directly closer to the target. As shown in Table 1, the angle at which each impulse force is directed is approximately 132 deg for all pulses, which corresponds to the angle from the uncontrolled impact point to the target. Figure 10 shows the evolution of projectile impact point with both the internal linear model prediction of impact point and the actual impact point for various numbers of control jets available. The agreement between the linear prediction and actual impact points is consistently good; in fact, it is within 2 ft for the impact points shown. This indicates that projectile linear theory provides an accurate estimate of the effect of each pulse on the impact point.

Typical dispersion results for the uncontrolled rocket and controlled rocket based on a sample of 50 trajectories are shown in Figs. 11 and 12. In both cases, the body pitch and yaw rates at rocket launch are taken to be independent normally distributed random variables with mean of −0.18 rad/s and zero, respectively, and standard deviations both equal to 0.3 rad/s. The aforementioned perturbations in initial angular rates are representative of launcher conditions that are known to cause dispersion. The controlled configuration has 12 2.25-lbf · s pulses and control laws optimized according to the case studies that follow. The circular error probable (CEP) in Figs. 11 and 12 is based on a 50% hit criterion, that is, the CEP is defined as the minimum radius of a circle centered at the mean impact point and containing at least 50% of the shot impact points. Figure 12 shows the distribution of impact points in

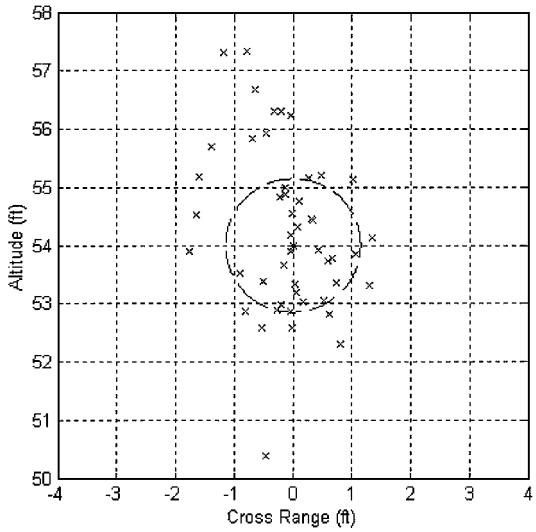

Fig. 12 Controlled dispersion (CEP = 1.15 ft).

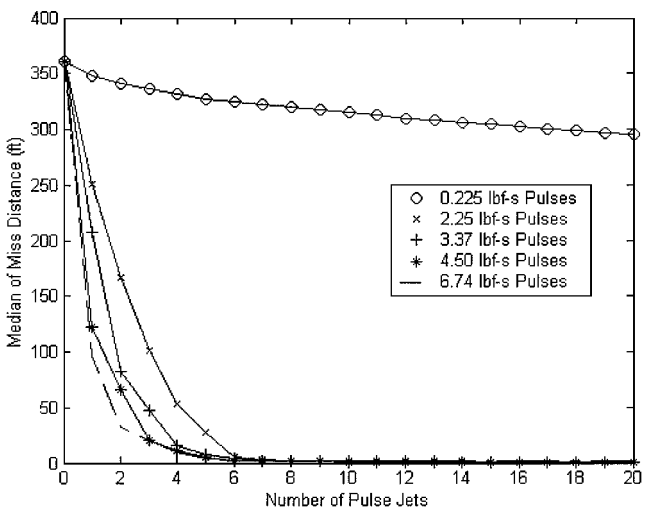

Fig. 13 Median miss distance vs number of pulse jets and impulse magnitude.

two dimensions for a sample of 50 trajectories. Note that Fig. 12 is zoomed in on the target to show the circle representing CEP and the impact points with miss distance equal to or less than the median. There are several outliers that fell outside of the zoomed axis boundaries. The nominal case of 12 pulses shows a phenomenal improvement from a CEP of 360.7 ft in the uncontrolled case to a CEP of 1.15 ft for the controlled case. Note also that an 80% hit criterion would increase the CEP circle to only 2.0189 ft. Also, the upper Kolmogorov band on the median is 1.7362 ft, indicating 95% confidence that the median of the population will be 1.7362 ft or less.

Figure 13 shows the median miss distance for different combinations of the number of pulse jets and the amplitude of each pulse jet. Lateral pulse jet arrays with larger individual pulse size cause a greater reduction in CEP when the total number of pulses available is eight or less. Arrays of six or more 2.25-lbf · s pulses or five or more 3.37-lbf · s and larger pulses are able to achieve a CEP of less than 5 ft. For a given lateral pulse jet control, Fig. 13 can be used to size the number and size of pulse jets in the pulse jet ring for a particular set of disturbances. Because the predictive flight control law requires several trajectory predictions in each sampling period, an important design parameter for the flight control system is the control system sampling period. Good pulse opportunities can be missed with too large a sampling inteval, whereas too small a sampling period may require an expensive sophisticated computer. Figure 14 shows the sensitivity of the predictive lateral pulse jet control law to control

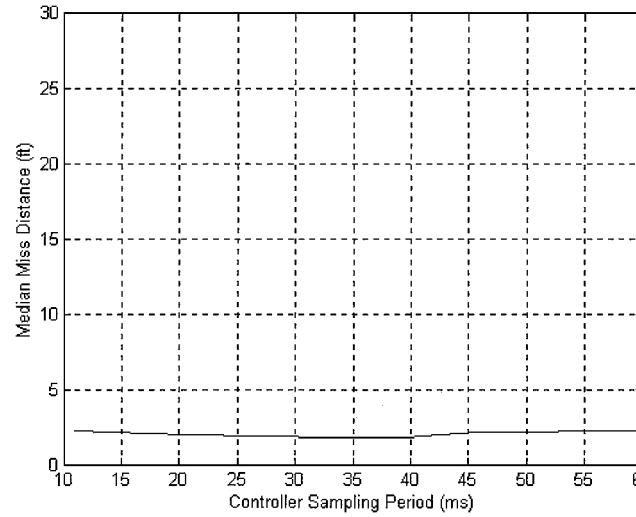

Fig. 14 Median miss distance vs controller sampling period.

system computational sampling period. For the range of sampling intervals shown, the median CEP is insensitive to sampling interval. These results are based on a fixed target. Note that, for a moving target, these results would need to be reexamined. Furthermore, the effect of target position update rate would need evaluation.

Conclusions

This paper develops a specialized control technique that blends model predictive control and projectile linear theory with a lateral pulse jet control mechanism. The methodology mates these system elements together in a natural way to form an efficient control system structure for this unique application. A three-dimensional trajectory control problem is converted to a two-dimensional control problem in the target plane by continuously mapping the state of the projectile to the target plane. The method directly focuses on controlling the impact point of the round. Prediction of the controlled and uncontrolled impact points is accomplished using a closed-form piecewise trajectory solution obtained using projectile linear theory. The linear theory trajectory solution permits rapid computation of the impact point, rendering the method practical for real-time implementation. By the use of a previously validated nonlinear projectile simulation, the control law is shown to reduce effectively impact point dispersion caused by disturbances at the launcher. For the example, rocket and pulse jet configuration are examined, and dispersion is reduced as the magnitude and number of pulse jets is increased. For thrusters with an impulse of 2.25 lbf · s or greater, a ring of eight pulse jets provides the majority of dispersion reduction. Rings with more individual thrusters decrease dispersion by a small amount. It is also found that dispersion is not significantly affected by the flight control law sampling interval. Although the dispersion reduction shown is quite substantial, these results should be tempered against error sources that add to dispersion characteristics of a fielded weapon system that were not included in the analysis, such as unknown atmospheric winds and IMU state estimation errors. Of course, impact point dispersion can only be reduced to the accuracy of the rocket position estimate in the vicinity of the target.

References

[1]Camacho, E., and Bordons, C., *Model Predictive Control*, Springer-Verlag, London, 1999, pp. 1–31.

[2]Murphy, C. H., "Symmetric Missile Dynamic Instabilities: A Survey," 18th AIAA Aerospace Sciences Meeting, Jan. 1980.

[3]Hodapp, A. E., "Effect of Mass Asymmetry on Ballistic Match of Projectiles," *Journal of Spacecraft and Rockets*, Vol. 13, No. 12, 1976, pp. 757–760.

[4]Weber, D. J., "Simplified Method for Evaluating the Flight Stability of Liquid-Filled Projectiles," *Journal of Spacecraft and Rockets*, Vol. 31, No. 1, 1994, pp. 130–134.

[5]Murphy, C. H., "Angular Motion of a Spinning Projectile with a Viscous Liquid Payload," *Journal of Guidance, Control, and Dynamics*, Vol. 6, No. 4, 1983, pp. 280–286.

[6]Cobb, K. K., Whyte, R. H., and Laird, P. K., "Effects of a Moving Components on the Motion of a 20-mm Projectile," *11th AIAA Aerodynamics Testing Conference*, AIAA, New York, 1983, pp. 94–103.

[7]Hodapp, A. E., "Passive Means for Stabilizing Projectiles with Partially Restrained Internal Members," *Journal of Guidance, Control, and Dynamics*, Vol. 12, No. 2, 1989, pp. 135–139.

[8]Soper, W. G., "Projectile Instability Produced by Internal Friction," *AIAA Journal*, Vol. 16, No. 1, 1978, pp. 8–11.

[9]Costello, M., and Peterson, A., "Linear Theory of a Dual-Spin Projectile in Atmospheric Flight," *Journal of Guidance, Control, and Dynamics*, Vol. 23, No. 5, 2000, pp. 789–797.

[10]Murphy, C. H., "Instability of Controlled Projectiles in Ascending or Descending Flight," *Journal of Guidance and Control*, Vol. 4, No. 1, 1981, pp. 66–69.

[11]Cooper, G., "Influence of Yaw Cards on the Yaw Growth of Spin Stabilized Projectiles," *Journal of Aircraft*, Vol. 38, No. 2, 2001, pp. 266–270.

[12]Guidos, B., and G., Cooper, "Closed-Form Solution of Finned Projectile Motion Subjected to a Simple In-Flight Lateral Impulse," AIAA Paper 2000-0767, 2000.

[13]Burchett, B., Peterson, A., and Costello, M., "Prediction of Swerving Motion of a Dual-Spin Projectile with Lateral Pulse Jets in Atmospheric Flight," *Mathematical and Computer Modeling*, Vol. 35, No. 1–2, 2002, pp. 1–14.

[14]Zarchan, P., *Tactical and Strategic Missile Guidance*, AIAA, Reston, VA, 1997.

[15]Pavlidis, T., "Optimal Control of Pulse Frequency Modulated Systems," *IEEE Transactions on Automatic Control,* Vol. AC-11, No. 4, 1966, pp. 676–684.

[16]Onyshko, S., and Noges, E., "Optimization of Pulse Frequency Modulated Control Systems via Modified Maximum Principle," *IEEE Transactions on Automatic Control*, Vol. AC-13, No. 2, 1968, pp. 144–149.

[17]VanderStoep, D. R., and Alexandro, F. J., "Bounds on the Optimal Performance of Pulse-Controlled Linear Systems," *IEEE Transactions on Automatic Control*, Vol. AC-13, No. 1, 1968, pp. 88–90.

[18]Nicoletti, B., and Raiconi, G., "A Computer Algorithm for the Optimization of Discrete-Time Pulse Frequency Modulated Systems," *IEEE Transactions on Automatic Control*, Vol. AC-19, No. 4, 1974, pp. 407–410.

[19]Onyshko, S., and Noges, E., "Pulse Frequency Modulation and Dynamic Programming," *IEEE Transactions on Automatic Control*, Vol. AC-14, No. 5, 1969, pp. 558–561.

[20]Elgazzar, S., and Onyshko, S., "Optimal Control Computation in Pulse Frequency Modulated Control Systems," *IEEE Transactions on Automatic Control*, Vol. AC-19, No. 4, 1974, pp. 452–454.

[21]Bennighof, J. K., Chang, S.-H. M., Subramaniam, M., "Minimum Time Pulse Response Based Control of Flexible Structures," *Journal of Guidance, Control, and Dynamics*, Vol. 16, No. 5, 1993, pp. 874–881.

[22]Bennighof, J. K., and Subramaniam, M., "Minimum Time Maneuver of Flexible Systems Using Pulse Response Based Control," *Journal of Guidance, Control, and Dynamics*, Vol. 20, No. 1, 1997, pp. 129–136.

[23]Singhose, W., Bohlke, K., and Seering, W., "Fuel-Efficient Pulse Command Profiles for Flexible Spacecraft," *Journal of Guidance, Control, and Dynamics*, Vol. 19, No. 4, 1996, pp. 954–960.

[24]Phillips, C. A., and Malyevac, D. S., "Pulse Motor Optimization via Mission Charts for an Exoatmospheric Interceptor," *Journal of Guidance, Control, and Dynamics*, Vol. 21, No. 4, 1998, pp. 611–617.

[25]Thurman, S., and Flashner, H., "New Pulse-Modulation Technique for Guidance and Control of Automated Spacecraft," *Journal of Guidance, Control, and Dynamics*, Vol. 19, No. 5, 1996, pp. 1007–1016.

[26]Thurman, S., and Flashner, H., "Robust Digital Autopilot Design for Spacecraft Equipped with Pulse-Operated Thrusters," *Journal of Guidance, Control, and Dynamics*, Vol. 19, No. 5, 1996, pp. 1047–1055.

[27]Bang, H., Park, Y., and Han, J., "Feedback Control for Slew Maneuver Using On–Off Thrusters," *Journal of Guidance, Control, and Dynamics*, Vol. 22, No. 6, 1999, pp. 816–822.

[28]Harkins, T. E., and Brown, T. G., "Using Active Damping as a Precision-Enhancing Technology for 2.75-Inch Rockets," U.S. Army Research Lab. ARL-TR-1772, Aberdeen Proving Ground, MD, 1999.

[29]Jitpraphai, T., and Costello, M., "Dispersion Reduction of a Direct Fire Rocket Using Lateral Pulse Jets," *Journal of Spacecraft and Rockets*, Vol. 38, No. 6, 2001, pp. 929–936.

[30]Etkin, B., *Dynamics of Atmospheric Flight*, Wiley, New York, 1972, Chap. 4.

[31]McCoy, R. L., *Modern Exterior Ballistics*, Schiffer Military History, Atglen, PA, 1999, pp. 221–244.

[32]Murphy, C. H., "Free Flight Motion of Symmetric Missiles," U.S. Army Ballistic Research Labs., BRL Rept. 1216, Aberdeen Proving Ground, MD, 1963.

[33]Costello, M., and Anderson, D., "Effect of Internal Mass Unbalance on the Terminal Accuracy and Stability of a Projectile," AIAA Paper 96-3447, 1996.

[34]Costello, M., and Peterson, A., "Linear Theory of a Dual Spin Projectile in Atmospheric Flight, U.S. Army Research Lab., TR, CR-448, Aberdeen Proving Ground, MD, Feb. 2000.